applied sciences

MDPI

Article

Empirical Mode Decomposition of Ultrasound Imagingfor Gain-Independent Measurement on Tissue Echogenicity: A Feasibility Study

Zhuhuang Zhou [1,2], Weiwei Wu [2], Shuicai Wu [1], Kebin Jia [2] and Po-Hsiang Tsui [3,4,5,*]

1 College of Life Science and Bioengineering, Beijing University of Technology, Beijing 100124, China; zhouzh@bjut.edu.cn (Z.Z.); wushuicai@bjut.edu.cn (S.W.)
2 Faculty of Information Technology, Beijing University of Technology, Beijing 100124, China; wuweiwei8889@163.com (W.W.); kebinj@bjut.edu.cn (K.J.)
3 Department of Medical Imaging and Radiological Sciences, College of Medicine, Chang Gung University, Taoyuan 33302, Taiwan
4 Medical Imaging Research Center, Institute for Radiological Research, Chang Gung University and Chang Gung Memorial Hospital at Linkou, Taoyuan 33302, Taiwan
5 Department of Medical Imaging and Intervention, Chang Gung Memorial Hospital at Linkou, Taoyuan 33305, Taiwan
* Correspondence: tsuiph@mail.cgu.edu.tw; Tel.: +886-3-211-8800 (ext. 3795)

Academic Editor: Dimitrios G. Aggelis
Received: 11 February 2017; Accepted: 22 March 2017; Published: 25 March 2017

Abstract: Empirical mode decomposition (EMD) is an adaptive method for decomposing a signal into intrinsic mode functions (IMFs).This study explored using EMD of ultrasound imaging for gain-independent measurements on tissue echogenicity. The IMF-based echogenicity ratio (IER) was proposed using the first (C_1) and second IMFs (C_2) of ultrasound radiofrequency data. Experiments on lipid phantoms were conducted to investigate the practical performance of IER. Phantoms with lipid concentrations 0%–30% (n = 36) were scanned using a clinical ultrasound scanner to acquire the radiofrequency data under different gains (12–33 dB) for EMD and IER calculations. Experiments on a tissue-mimicking phantom were further performed using the same ultrasound system and data acquisition procedure to investigate the effect of ultrasound frequency on the IER at5–8 MHz.Experimental results showed that the IER measured under 33-dB gain decreased from 6.65 ± 0.23 to 3.97 ± 0.10 when the lipid concentrations were increased from 0% to 30%. When 12-dB gain was used, the IER decreased from 6.21 ± 0.29 to 3.39 ± 0.07. However, whenincreasing the frequency, the IER had a mean decreasing rate of -8.67% per MHz, which was lower than those of the C_1 and C_2 intensities.The proposed IER may allow gain-independent measurement on tissue echogenicity.

Keywords: empirical mode decomposition; intrinsic mode function; echogenicity

1. Introduction

Ultrasound imaging is an essential clinical tool for screening tissue structures. The intensity of an ultrasound grayscale image (B-mode) is determined based on the amplitude of the backscattered signals resulting from the interactions between acoustic scatterers and the incident wave. When the degree of an acoustic impedance mismatch is increased, the signal amplitude and the corresponding B-scan brightness increase accordingly. In clinical settings, B-scan brightness is generally used to describe the echogenicities of the scatterers in a tissue for diagnosis. Although several functional imaging techniques are available in current ultrasound systems, the conventional B-scan is still widely adopted as a convenient screening tool for describing echogenicity in clinical evaluation [1–5], because

diseases typically accompany changes in acoustic properties of scatterers in tissues (e.g., liver steatosis or muscle fibrosis) [3–5].

In addition to the effects of an acoustic impedance mismatch, the brightness of B-scans depends on system factors such as system gain, time gain compensation (TGC), log compression, and signal/image processing; among these, system gain is a dominant factor for determining the amplitudes of received signals and the corresponding image brightness. The most frequent problem in clinical settings entails different users using different gains for screening, thus resulting in varied explanations for the echogenicity of examined tissues. In some conditions, the above problem may be overcome by normalizing the intensity with the background image data (e.g., liver-to-kidney intensity ratio for fatty liver assessment). However, for different types of tissues, it is not necessary to have appropriate background information that can be used for normalization. This might explain why researchers cannot reach a definitive diagnosis when using B-scans alone. Thus, establishing an objective index or a measurement protocol that is independent of the system gain is essential when describing tissue echogenicity by using B-scans in routine clinical examinations. However, no relevant studies have explored this concern. This paper addresses the following fundamental question: Can the image intensity measure be independent of the system gain?

Understanding the ultrasound backscattered signal model may be an effective foundation for answering the posed question. Previous studies have described that under ideal conditions, ultrasound backscattered signals $s(t)$ can be modeled as a result of the convolution of the incident wave with the tissue function [6–8],

$$s(t) = h(t) \otimes z(t) \tag{1}$$

where $h(t)$ represents the transfer function of the transducer (i.e., the incident wave), and $z(t)$ denotes the spatial distribution function of the scatterers. After amplification by using an ultrasound system, the following equation is obtained:

$$s(t) = G \times [h(t) \otimes z(t)] \tag{2}$$

where G denotes the system gain. Apparently, a gain effect was intrinsic to the signals output from a system and therefore unavoidable. We assume that signal processing based on self-decomposition and normalization may provide an effective solution to eliminating the gain effect from the ultrasound echo measurements. The reason is explained as follows. Signal self-decomposition produces several sub-signals with the same gain effect, and these sub-signals can be used for normalization to eliminate the gain effect. In the meantime, the signal normalization results must contain physical meanings associated with $h(t)$ and $z(t)$ to enable describing the tissue echogenicity. Therefore, selecting an appropriate decomposition method for signal normalization may be critical to satisfy these requirements.

Recently, the Hilbert-Huang Transform (HHT) has become a highly attractive time-frequency analysis method for nonlinear and non-stationary data [9–12]. In the HHT, an empirical mode decomposition (EMD) was developed for meaningfully determining the instantaneous frequency of a signal. When EMD is used, a signal can be decomposed into a set of intrinsic mode functions (IMFs) for calculating the instantaneous frequencies through the HHT. In particular, the advantage of EMD over other signal decomposition methods (e.g., wavelet) is that EMD requires no signal base for signal decomposition; therefore, a signal can be adaptively decomposed into n empirical modes. The gain effect exists in each IMF component produced from the EMD of the ultrasound signals, and thus it may be eliminated using various IMFs for signal normalization. Note that the above assumption has been preliminarily validated by experiments on newly-formed and aged thrombi [13]. In the current stage, three fundamental issues need to be further clarified: (i) the proposed idea needs to be demonstrated theoretically; (ii) different system gains result in different signal-to-noise ratios (SNRs). The effects of SNR on the proposed method should be explored; and (iii) considering that the factors G,

$h(t)$, and $z(t)$ are essentially functions of ultrasound frequency, the frequency effect on the proposed method also needs to be investigated.

To address the feasibility of using EMD as an adaptive strategy forestablishing a gain-independent index for describing tissue echogenicity, in the subsequent sections we review the principles of EMD and present an ultrasound signal model to theoretically demonstrate that the gain effect can be eliminated by signal normalization using the IMFs. We then define an echogenicity index based on using the IMFs to validate its performance in quantifying the image intensity of ultrasound B-scans under various system gains (i.e., signal-to-noise ratios [SNRs]) and explore its dependency of ultrasound frequency. Finally, we discuss the potential impacts of using the proposed method in future applications.

2. Theory

EMD is a key constituent of the HHT, an adaptive time-frequency analysis method for nonlinear and non-stationary data. Previous studies have described the HHT in detail [9,10]. Here, we briefly explain how to perform the EMD.

First, we determine the local maxima and minima of a signal $x(t)$ and use cubic spline interpolation to obtain its upper and lower envelopes. If the mean of these two envelopes is $d_1(t)$, then the difference between the signal and $d_1(t)$ is the first component $h_1(t)$:

$$h_1(t) = x(t) - d_1(t). \tag{3}$$

This is called the sifting process. To determine whether $h_1(t)$ is an IMF, it must be a single-component signal that fulfills the following conditions: (i) the number of zero crossings and extrema must be no more than one forthe entire data set; and (ii) the mean value of the upper and lower envelopes, which are defined using the local maxima and minima, respectively, is zero at any time, meaning that the two envelope curves are symmetric about the time axis. Ideally, when the cubic spline interpolation is perfect, with no gentle hump on the signal slope, $h_1(t)$ must satisfy the IMF requirements. However, imperfect fitting commonly produces overshoots and undershoots that generate new extrema and shift or exaggerate existing ones. Even when the fitting is perfect, humps may become local extrema after the first round of sifting. Moreover, the envelope mean may differ from the true local mean of the signal for non-stationary data, resulting in an asymmetric waveform. Therefore, the sifting process must be repeated k times until the extracted difference is an IMF. In the second iteration, $h_1(t)$ is treated as the original data in the second sifting process:

$$h_1(t) - d_{11}(t) = h_{11}(t). \tag{4}$$

The sifting process is repeated k times until $h_{1k}(t)$ is determined, which is an IMF:

$$h_{1(k-1)}(t) - d_{1k}(t) = h_{1k}(t). \tag{5}$$

Then, we define

$$C_1(t) = h_{1k}(t) \tag{6}$$

as the first IMF component (i.e., component C_1) for the data. Overall, C_1 contains the finest and shortest period component of the signal. Subsequently, we can subtract $C_1(t)$ from the signal:

$$x(t) - C_1(t) = r_1(t). \tag{7}$$

Because residue $r_1(t)$ still contains information about the components with longer periods, we consider it new original data and apply the same aforementioned sifting process. This procedure can be repeated for all subsequent $r_j(t)$ values, yielding

$$r_1(t) - C_2(t) = r_2(t), \ldots, r_{n-1}(t) - C_n(t) = r_n(t). \quad (8)$$

Summing Equations (6)–(8) ultimately yields

$$x(t) = \sum_{i=1}^{n} C_i(t) + r_n(t). \quad (9)$$

This indicates that $x(t)$ is decomposed by EMD into n IMFs (C_1, C_2, C_3, ... , C_i, from high-frequency to low-frequency components) and a residue $r_n(t)$, which is the signal trend with a maximum of one extremum or a constant.

3. Materials and Methods

Three parts are organized in this section. First, mathematical demonstrations were used to confirm the feasibility of developing a gain-independent index based on EMD for describing tissue echogenicity, and computer simulations were performed for validations of mathematical equations. Second, experiments on lipid phantoms were carried out to explore the ability of the gain-independent index to describeechogenicity under different gains. Third, experiments on a tissue-mimicking phantom were performed to investigate the effect of ultrasound frequency on the proposed gain-independent index in a more realistic condition.

3.1. Theoretical Demonstration

According to the properties of EMD, the ultrasound backscattered data $s(t)$ can be decomposed into numerous IMFs expressed as follows:

$$s(t) = s_1(t) + s_2(t) + \ldots\ldots + s_n(t). \quad (10)$$

We assume that the incident wave of ultrasound $h(t)$ can be decomposed by the EMD, and then we can obtain the following:

$$h(t) = h_1(t) + h_2(t) + \ldots\ldots + h_n(t). \quad (11)$$

According to Equation (2), we can obtain the following:

$$s_1(t) = G \times [h_1(t) \otimes z(t)],\ s_2(t) = G \times [h_2(t) \otimes z(t)],\ ...,\ s_n(t) = G \times [h_n(t) \otimes z(t)]. \quad (12)$$

Summing all the signals in Equation (12), we can obtain the following:

$$\begin{aligned} s_1(t) + s_2(t) + \ldots\ldots s_n(t) &= G \times [h_1(t) \otimes z(t)] + G \times [h_2(t) \otimes z(t)] + ... + G \times [h_n(t) \otimes z(t)] \\ &= G \times [h_1(t) \otimes z(t) + h_2(t) \otimes z(t) + ... + h_n(t) \otimes z(t)] \\ &= G \times [(h_1(t) + h_2(t) + ... + h_n(t)) \otimes z(t)] \\ &= G \times [h(t) \otimes z(t)] \\ &= s(t) \end{aligned} \quad (13)$$

Notably, Equation (13) appears to be an inverse demonstration of Equation (10), indicating the following properties: (i) summing $s_1(t)$, $s_2(t)$, ... , $s_n(t)$ can reconstruct the original backscattered signal $s(t)$; (ii) the incident wave $h(t)$ can be decomposed into $h_1(t)$, $h_2(t)$, ... , $h_n(t)$, which can be further treated as the incident ultrasound waves with different frequency components; and (iii) the IMFs of the backscattered signals [$s_1(t)$, $s_2(t)$, ... , $s_n(t)$] are the echo signals generated by the transmitting incident waves $h_1(t)$, $h_2(t)$, ... , $h_n(t)$ into the tissue $z(t)$ for interactions. In this condition, two arbitrary IMFs of the backscattered signal can be further used for normalization. For ultrasound signals, higher-frequency IMFs have larger signal amplitudes and relevant physical meanings [14].

In particular, the amplitude of the third IMF starts to be smaller than 10% of that of the original backscattered signals [14], and thus the IMFs from C_3 to C_n may not be the primary components of the signals. For the above reasons, an IMF-based echogenicity ratio (IER) was defined using the first and second IMFs of the backscattered signals for signal normalization:

$$IER = \frac{s_1(t)}{s_2(t)} = \frac{G \times [h_1(t) \otimes z(t)]}{G \times [h_2(t) \otimes z(t)]} = \frac{h_1(t) \otimes z(t)}{h_2(t) \otimes z(t)}. \quad (14)$$

In practice, the IER is calculated using the ratio of the envelope amplitude of the first IMF to that of the second IMF. Ideally, the calculation of the IER allows self-normalization of the signal, which produces a gain-independent index that is associated with $h(t)$ and $z(t)$. This suggests the presence of a correlation between the IER and the B-scan intensity.

To confirm the proposed equations, one-dimensional computer simulations were performed for validations. A 5-MHzGaussian pulse with a bandwidth of 60% was generated as the incident wave $h(t)$. A computer phantom $z(t)$ with a concentration of 32 scatterers/mm^3 was constructed by a sequence with randomly positioned delta functions. The sampling rate was 100 MHz. Gain factors G of 5, 10 and 20 were set. The ultrasound backscattered signals $s(t)$ were then obtained using Equation (2).

3.2. Experiments on Lipid Phantoms

Experiments on phantoms with different behaviors of echogenicity were performed. The phantom was prepared by boiling the agar-water mixture (dissolving 1.5 g of agar powder in 200 mL of water) and cooling it to form a solid gel. The graphite powder with <20-μm particles (Model 282863, Sigma-Aldrich, St. Louis, MO, USA) was added to the phantom to simulate the scatterers in tissue. The number density of the scatterers in the phantom was 128 scatterers/mm^3, which was adequately large to produce a fully developed speckle pattern in a B-mode image. To further produce different image intensities of the B-scan, various proportions of soybean-oil lipid emulsion (Intrafat, Nihon Pharmaceutical Industry, Osaka, Japan) were added to the phantoms to produce varying degrees of attenuation, as presented in Figure 1a,b. The lipid concentrations ranged from 0% to 30%, corresponding to the range of attenuation coefficient from 0.684 to 1.108 dB/cm·MHz (the attenuation coefficient of each phantom was calculated using the standard substitution method). A previous study reported that when the lipid concentrations are increased, the brightness of the B-scan decreases accordingly [15]. In total, six independent phantoms were prepared for each lipid concentration (n = 36).

A commercial ultrasound scanner (Model 3000, Terason, Burlington, MA, USA) was used to scan the phantoms. The applied probe was a wideband linear array with a central frequency of 7 MHz and 128 elements (Model 10L5, Terason). An agar phantom with the same graphite powder concentrations was prepared to calibrate the gain setting in the imaging system. A cyst was created as an anechoic region in the center of the phantom, and the image intensities, calculated using the square of the envelope amplitude, corresponding to the cyst and the phantom background were used to estimate the SNRs, as shown in Figure 1c. The calibration results obtained from six independent measurements are shown in Figure 1d. When the digital gain index in the system was adjusted from 1 to 6, the SNRs produced ranged from 12 to 33 dB, which was used as the range of gain applied to the phantom scanning.

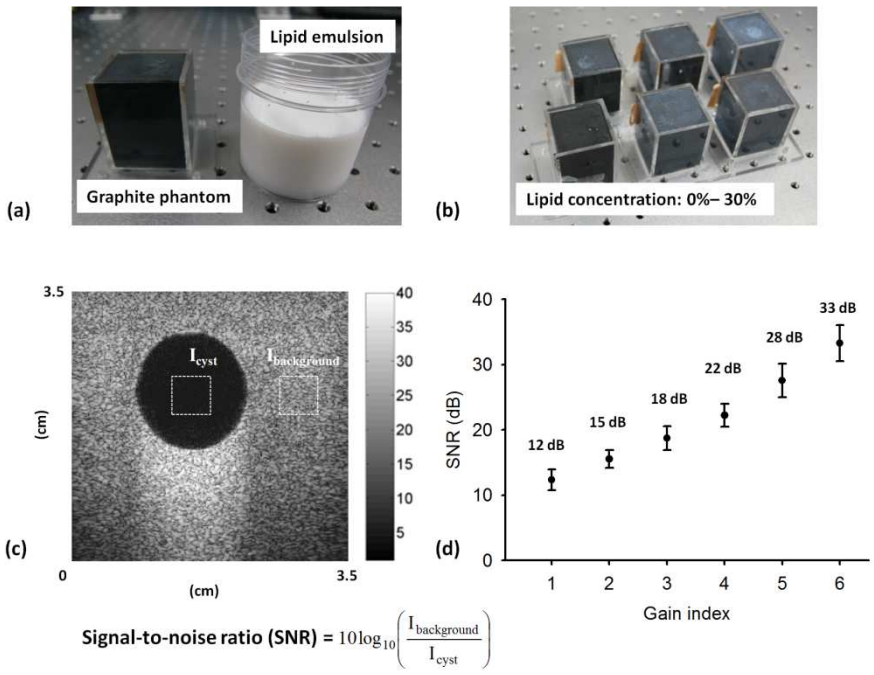

Figure 1. Phantoms (**a**,**b**) were prepared using graphite powder. To produce different image intensities of the B-scan, various proportions of soybean-oil lipid emulsions (0%–30%) were added to the phantoms to produce varying degrees of attenuation; (**c**) B-mode image of the cyst phantom that was used for calibrating the system gain; (**d**) The signal-to-noise ratio (SNR) that was used to represent the gain increase from 12 to 33 dB when the digital gain index in the system increased from 1 to 6.

Each lipid phantom was immersed in a water tank and scanned using the ultrasound system with different system gains that ranged from 12 to 33 dB. The image raw beamformed radiofrequency (RF) data were acquired from the phantom at a 30-MHz sampling rate. In total, the image comprised 128 scan lines of the backscattered echoes, corresponding to a size of 3 × 3.5 cm (depth × width). The image scan lines were demodulated using the absolute value of the Hilbert transform to obtain the envelope image, which was then normalized and compressed using logarithmic calculations to obtain the B-mode image at a dynamic range of 40 dB (i.e., the pixel values range between 0 and 40 dB). Concurrently, the raw RF image data were decomposed into the IMFs by using a two-dimensional (2D) EMD, which was developed by Wu et al. [16] for image EMD processing. After applying 2D EMD on the RF signals, each IMF signal was demodulated and log-compressed to display the IMF-based B-mode images (i.e., C_1, C_2, ... , C_i images). Based on Equation (14), we selected a 1×1cmsizedregion of interest (ROI) to calculate the average image intensities(the square of the envelope amplitude) of the C_1 and C_2 images for calculating the IER, as shown in Figure 2. The relationships among these values (C_1 intensity, C_2 intensity, and IER), gain, and lipid concentrations were compared to evaluate the performance of the proposed IER parameter in describing the tissue echogenicity.To evaluate the tolerance of the proposed method to the gain setting, the measurement errors of the C_1 intensity, C_2 intensity, and IERwere estimated using the following:

$$Measurement\ error = \left| \frac{x - \overline{x}_{(33\text{dB})}}{\overline{x}_{(33\text{dB})}} \right| \times 100\%, \tag{15}$$

where x means the individual intensity value of C_1, C_2, and IER, and $\overline{x}_{(33\text{dB})}$ represents the average value at the maximum gain obtained from six phantoms.

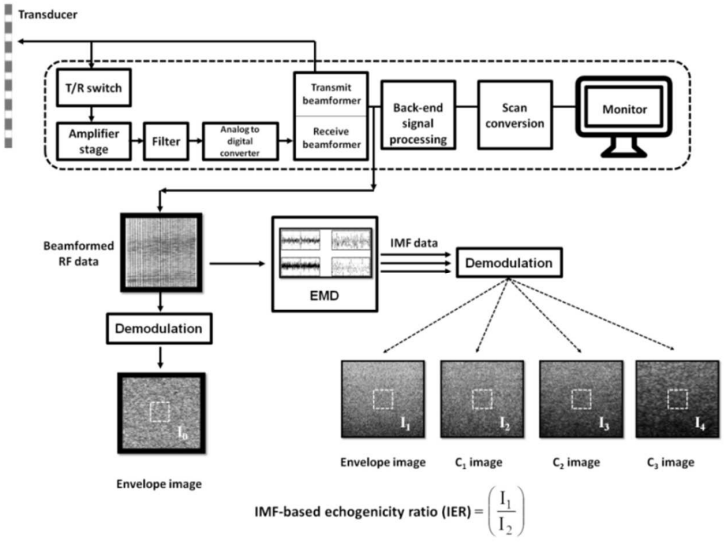

Figure 2. Illustration to explain the intrinsic mode functions (IMF) based echogenicity ratio (IER) calculation. The raw RF image data were decomposed into the IMFs) by using the 2D empirical mode decomposition (EMD). Higher-frequency IMFs exhibit larger signal amplitudes and relevant physical meanings; thus, IER was defined using the first (C_1) and second (C_2) IMFs for signal normalization.

3.3. Experiments on a Tissue-Mimicking Phantom

A tissue-mimicking breast phantom (Model BPB170, Blue Phantom, Redmond, WA, USA) was used to provide a simulated mass, as shown in Figure 3. Five independent scans of the simulated mass were performed using the same Terason ultrasound scanner and the transducer. For each scan, the transmitting central frequency was set at approximately 5, 5.5, 6, 7.5 and 8 MHz by using the software development kit to acquire image RF data corresponding to different frequencies. The RF data comprised 128 scan lines of the backscattered echoes, corresponding to a size of 3.5 × 3.5 cm (depth × width). The same procedures as mentioned in the previous subsection were used to obtain the B-mode and IMF-based images. For each image, a ROI with a size of 5×5mm was located in the mass to calculate the average intensities of the C_1 and C_2 images for calculating the IER. The image intensities (C_1 and C_2) and the IER as functions of frequency were plotted for comparison.

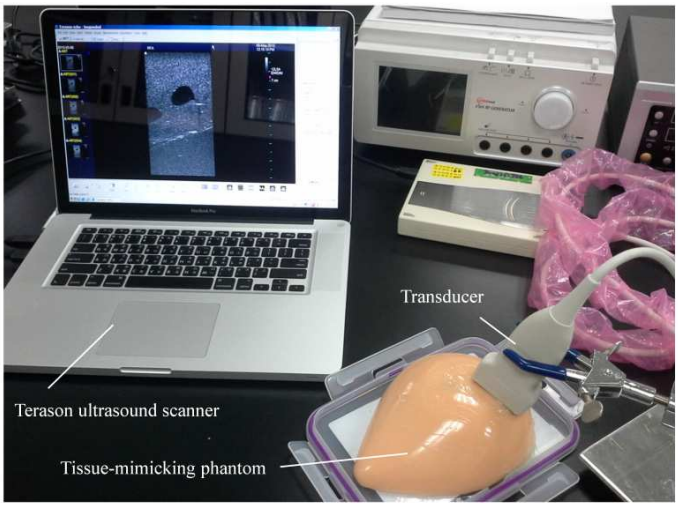

Figure 3. The experimental setup for imaging the tissue-mimicking breast phantom using the commercial ultrasound scanner.

4. Results

Figure 4 shows the backscattered signals $s(t)$ with different gain factors obtained from simulations and the corresponding IMFs after applying EMD of $s(t)$. In practice, the ratios of amplitude between different IMFs may depend on the degree of noise interference on the signal. However, while using the raw backscattered signals without any postprocessing for EMD, the primary components of the original signals were assigned to the first and second IMFs. The quantitative analysis of the signals showed that the C_1 and C_2 account for up to 90% of the amplitude of the backscattered signals, as shown in Figure 5. This finding agreed well with the previous study [14], supporting the selection of C_1 and C_2 for the definition of the IER. Moreover, the results in Figure 4 further showed that the summation of each IMF multiplied by the gain factor equals the signal multiplied using the same gain, demonstrating the reasonability of Equations (12) and (13).

Figure 6a–f present the B-mode images and the corresponding C_1, C_2, C_3, and C_4 images of the phantoms with varied lipid concentrations ranging from 0% to 30%. The speckle patterns in the B-mode images of different phantoms were similar because the number density of the scatterers in each phantom was set the same.For each lipid concentration, the speckle pattern of the C_1 image was similar to that of the B-mode image. Notably, the EMD decomposed image data to produce the IMFs from high- to low-frequency components. The first IMF was the data with the highest-frequency components compared with the other IMFs; therefore, the signal waveforms in the C_1 image were similar to those of the original backscattered RF echoes but more symmetrical in the upper and lower envelopes [14,17]. This also explains why the other IMF-based images (C_2, C_3 and C_4 images in Figure 6) exhibited poorer spatial resolutions compared with the C_1 image.

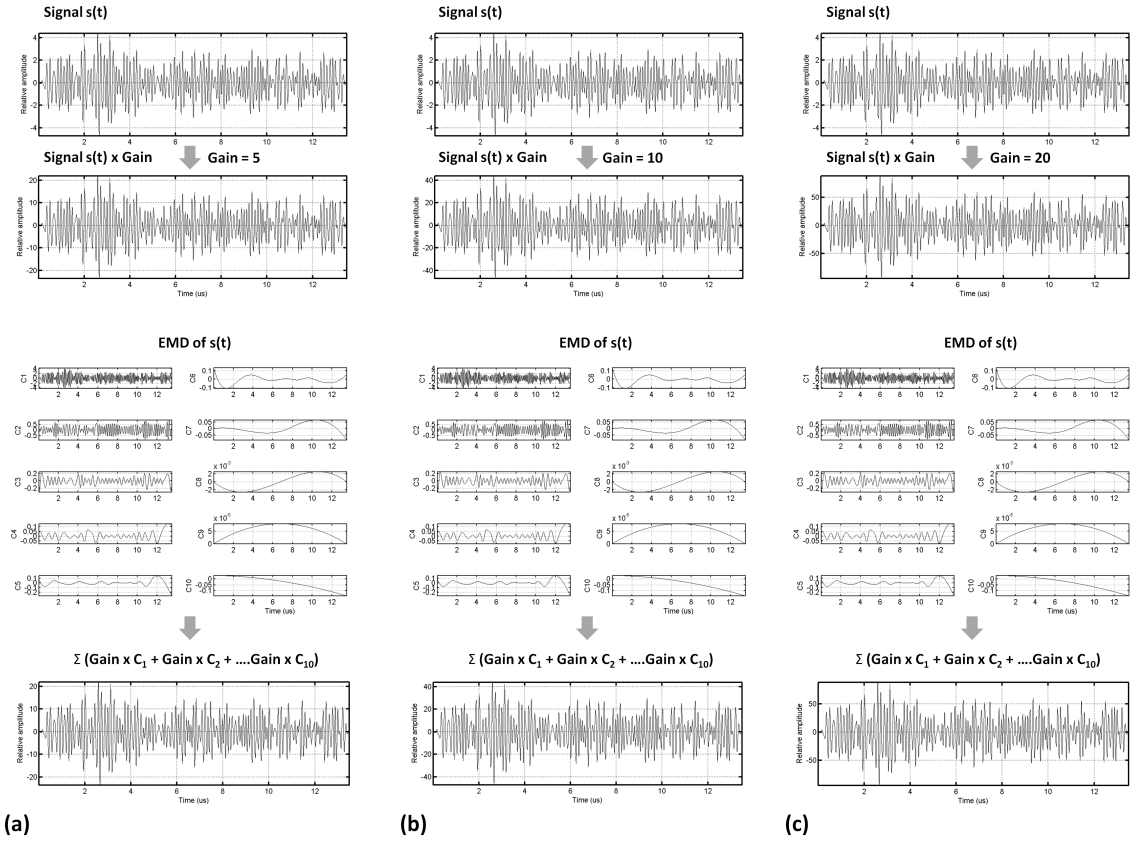

Figure 4. The backscattered signals $s(t)$ with different gain factors obtained from simulations and the corresponding IMFs after applying EMD of $s(t)$. The summation of each IMF multiplied by the gain factor equals the signal multiplied using the same gain factor.

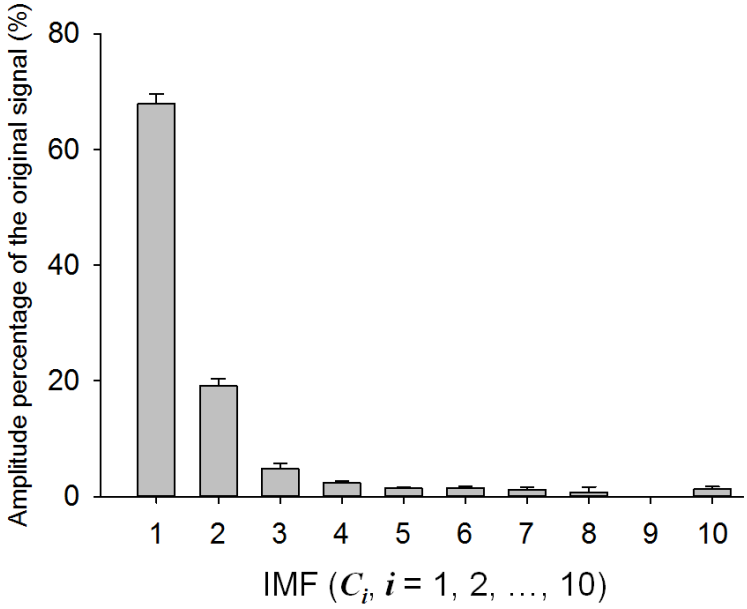

Figure 5. The percentage of amplitude of each IMF compared with that of the original backscattered signal (obtained from ten independent simulations). The first and second IMFs account for up to 90% of the amplitude of the backscattered signals.

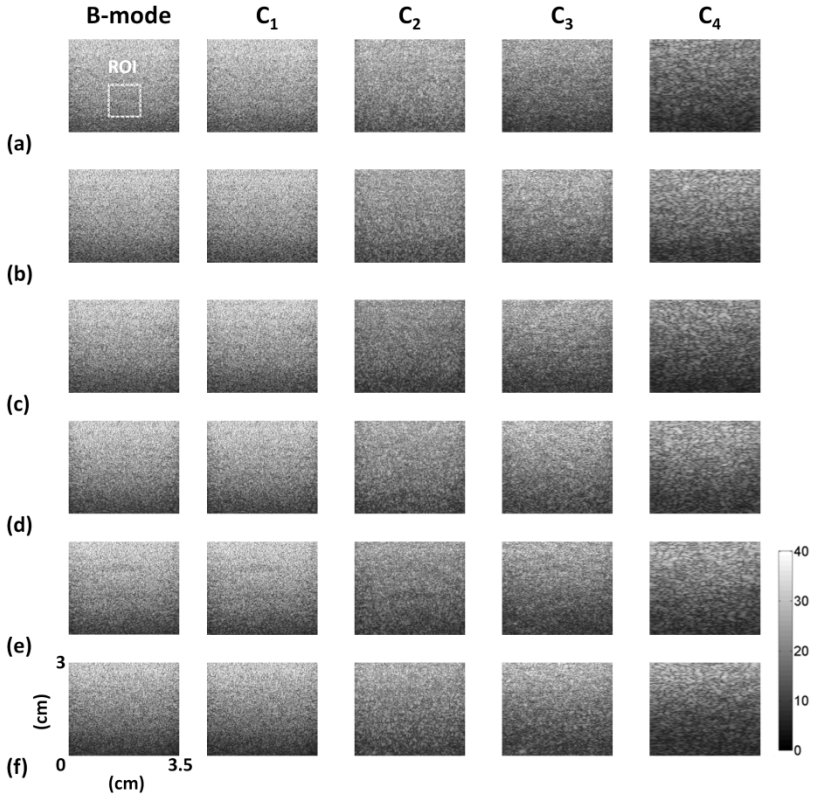

Figure 6. B-mode and C_1–C_4 images of the phantoms with lipid concentrations ranging from 0% to 30%. (**a**) 0%, (**b**) 5%, (**c**) 10%, (**d**) 15%, (**e**) 20% and (**f**) 30%. B-mode and IMF-based images are constructed using the log-compressed envelopes of the RF and IMF data obtained from the EMD. ROI: region of interest.

The C_1 image intensities were observed as a function of the lipid concentrations obtained using gains ranging from 12 to 33 dB (Figure 7a). At 33-dB gain, the C_1 intensity decreased from 185.89 ± 19.74 to 61.91 ± 3.09 when the lipid concentrations were increased. Because of the extreme resemblance between the C_1 and the RF signals, the C_1 image intensity could be considered as that measured using the RF data. When the gain decreased to 12 dB, the C_1 intensity decreased from 76.31 ± 7.72 to 26.46 ± 1.12 in the same range of lipid concentrations. As shown in Figure 7b, when the system gain decreased to 12 dB, the average error for the various lipid concentrations was larger than 50%. Note that the C_1 image findings were also observed in the C_2 image, as shown in Figure 7c,d. The C_2 intensities measured using 33 and 12 dB decreased from 27.92 ± 2.59 to 15.58 ± 0.56 and from 12.26 ± 0.94 to 7.78 ± 0.27, respectively; the measurement error at 12 dB was also >50%. These results demonstrated that the intensity measurement was significantlyaffected by the gain effect. Figure 7e displays the IERs as a function of the lipid concentrations at different system gains. The IERs measured using 33 and 12 dB decreased from 6.65 ± 0.23 to 3.97 ± 0.10 and from 6.21 ± 0.29 to 3.39 ± 0.07, respectively, when the lipid concentrations were increased from 0% to 30%, respectively. Evidently, the proposed IER largely reduces the dependency of intensity measurement on the system gain factor and the measurement error, as shown in Figure 7f.

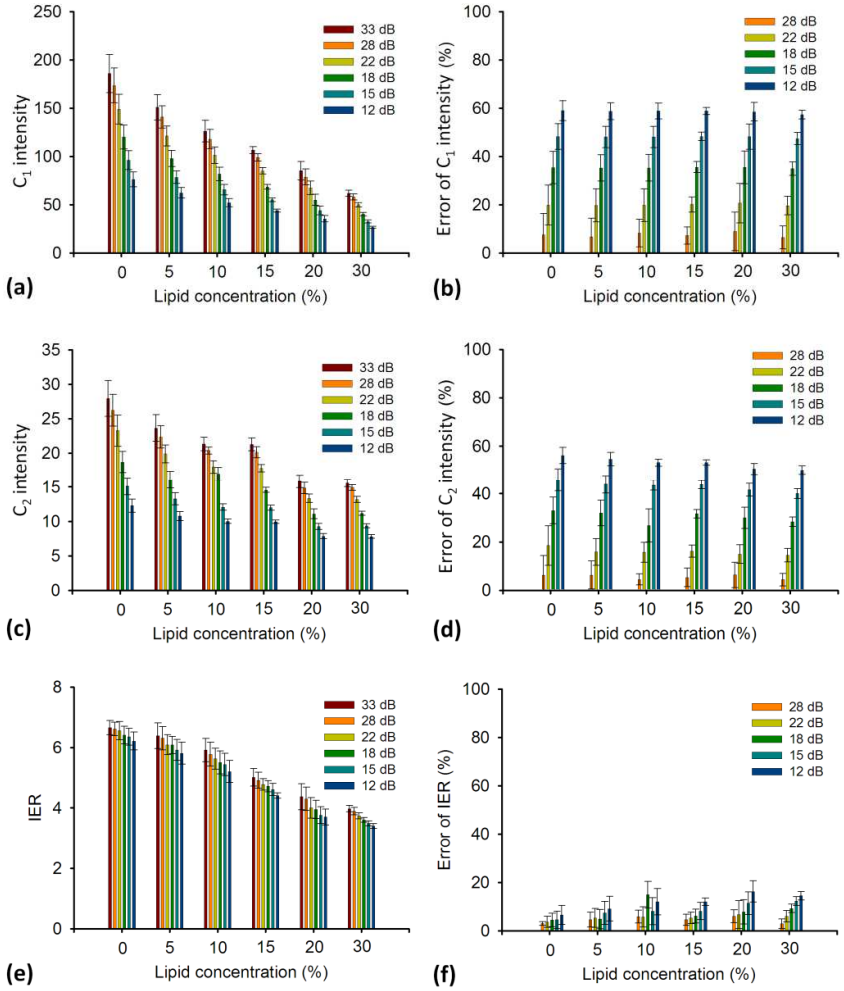

Figure 7. Results of the EMD-based parameters as a function of lipid concentration obtained at various system gains. (**a**) C_1 image intensity; (**b**) Measurement error forthe C_1 intensity; (**c**) C_2 image intensity; (**d**) Measurement error forthe C_2 intensity; (**e**) IER; (**f**) Measurement error forthe IER. The results indicated that the IER is less affected by the system gain because its measurement error is much lower than the errors forthe C_1 and C_2 data.

In particular, we found that the measurement errors further decreased when the gain increased, as shown in Figure 8. Figure 9 shows the B-mode and the corresponding C_1 and C_2 images of the simulated mass measured using different ultrasound frequencies. With an increaseinfrequency, the speckle patterns became more meticulous, resulting in an improved spatial resolution of theimage. The quantitative analysis of the image intensity and the IER as a function of ultrasound frequency is shown in Figure 10. The C_1 intensity decreased from 48.6 $\pm$ 6.94 to 24.2 $\pm$ 1.08 when the ultrasound frequency increased from 5 to 8 MHz, corresponding to a mean decreasing rate of -16.67% per MHz. Forthe same frequency range, the C_2 intensity decreased from 10.1 $\pm$ 0.70 to 6.41 $\pm$ 0.29 with a mean decreasing rate of -11.67% per MHz. Compared to the C_1 and C_2 intensities, the IER decreased from 4.90 $\pm$ 0.93 to 3.78 $\pm$ 1.33 in accordance with a mean decreasing rate of -8.67% per MHz.

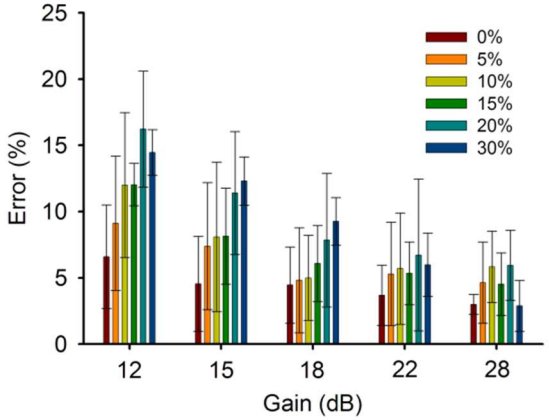

Figure 8. Measurement error as a function of system gain for various lipid concentrations. The measurement error decreases when the system gain increases. A higher gain is suggested to improve the measurement error of the IER.

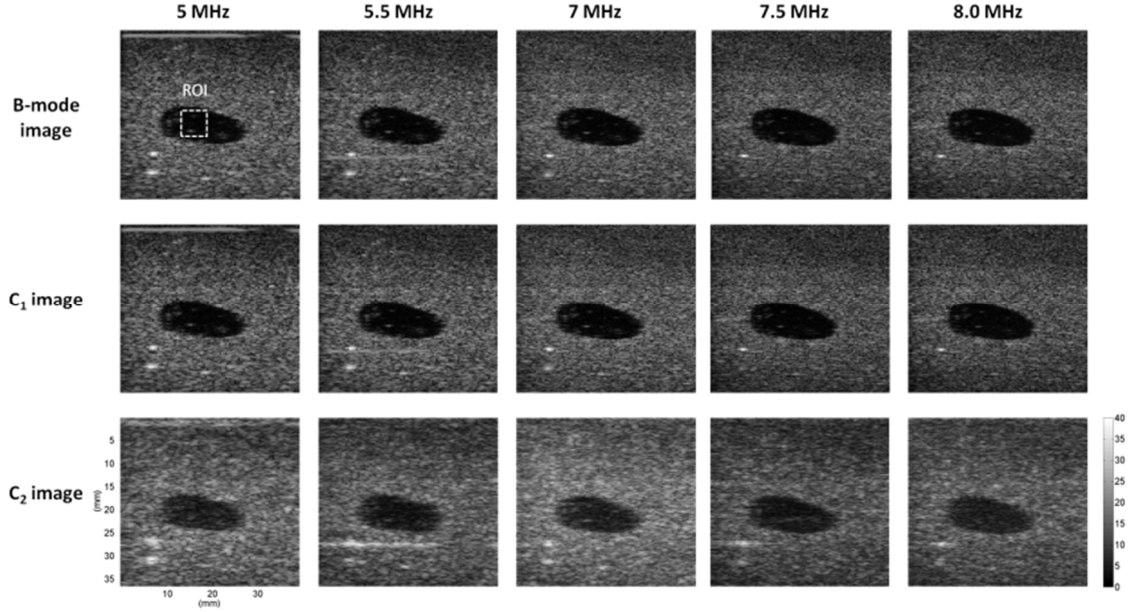

Figure 9. The B-mode and the corresponding C_1 and C_2 images of the simulated mass measured using different ultrasound frequencies from 5 to 8 MHz. ROI: region of interest.

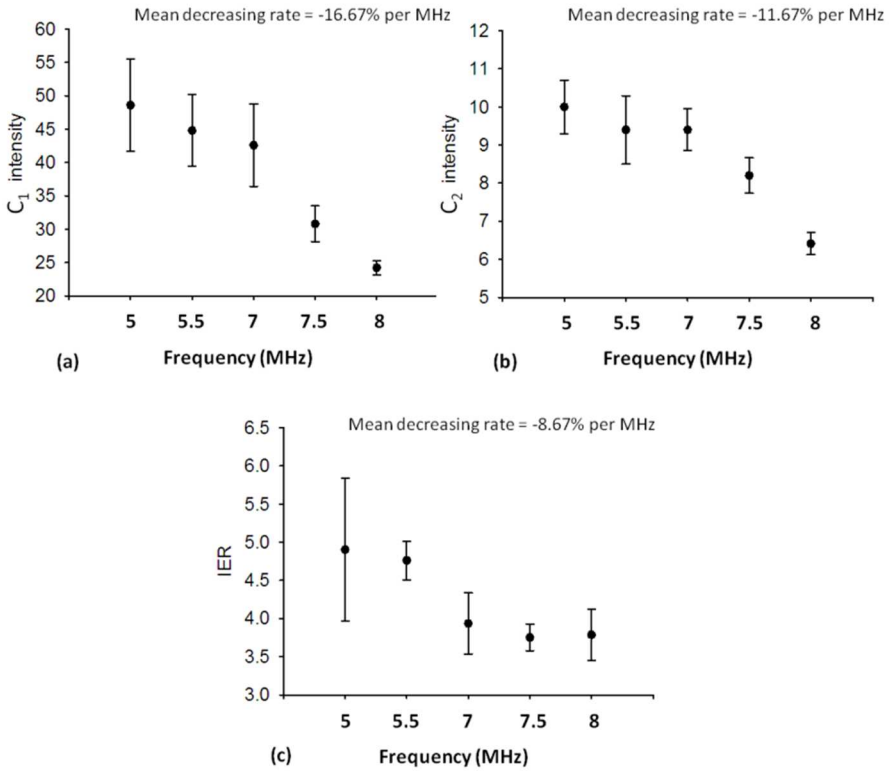

Figure 10. The image intensities of C_1 (**a**) and C_2 (**b**) modes and the IER (**c**) as a function of ultrasound frequency. Whenincreasing the frequency, the IER had a mean decreasing rate of −8.67% per MHz, which was lower than those of the C_1 and C_2 intensities.

5. Discussion

This study used EMD as a strategy to develop a gain-independent index for describing the echogenicity of a scattering medium. An ideal echo model was used to concord with the EMD properties to demonstrate theoretically the feasibility of the proposed hypothesis. The current experimental results obtained from the phantoms demonstrated that the proposed IER maybe less affected by the gain setting. EMD has been widely applied in resolving several engineering and scientific problems [18]. Increasingly, more studies have investigated EMD applications in the field of medical ultrasound imaging, including tissue harmonic imaging [17], signal filtering [19], improvements in tissue characterization by using statistical parameters [20,21], image contrast enhancement [22,23], and elastography construction [24].This study is the first to explain how EMD eliminates the effects of the system gain from echogenicity measurement.

In this study, the IER was defined using the C_1 and C_2 of the backscattered signals. Thecurrent findings and explanations are summarized below to support the proposed method: (i) referring to the schematic of an ultrasound imaging system (Figure 2), ultrasound echo signals are received by a transducer with a specific bandwidth. The received signals are subsequently amplified using the same amplifier stage with a passband that is typically designed to overlap with the transducer bandwidth for amplifying the signals with the same gain; (ii) the results showed that the C_1 and C_2 account for up to 90% of the amplitude of the backscattered signals, demonstrating that the first and second IMFs are the primary components of the original signals; and (iii) the summation of each IMF multiplied by the gain factor equals the signal multiplied using the same gain. For these reasons, it is convincing to define the IER using the first and second IMFs based on the proposed Equations (12) and (13).

It is interesting to discuss the physical meanings of the IER. As indicated in Figure 7, the C_1 and C_2 intensities decreased as the lipid concentrations were increased. This is because when the lipid emulsion concentration increases, the phantom increases the attenuation effects to reduce the echo

intensity [15]. It should be noted that the IER also decreased as the lipid concentrations were increased. Comparing the results in Figure 7 suggests a considerable difference in the sensitivities of C_1 and C_2 intensities to respond to variations in the lipid concentrations. The first C_1 IMF adequately follows the form of the original ultrasound signal and is the highest-frequency component [17]. Because the attenuation effect is proportional to the signal frequency, the C_1 signal intensity may be more sensitive to the attenuation effect and may thus weaken in a high-attenuation scattering medium. Although the C_2 intensity decreases as the attenuation effect increases, the influence of attenuation on the signal intensity is relatively weaker because the C_2 IMF is a relatively low-frequency signal. In other words, the IER not only depends on the backscattered intensity but also correlates with the effect of ultrasound frequency.

As mentioned in Introduction, the factors G, $h(t)$, and $z(t)$ are functions of frequency. In modern ultrasound systems, the frequency effect of the system gain G may be ignored because wideband electronic amplifiers are typically used in circuits to ensure that the frequency-independent passbands in the Bode Plots of the amplifiers can cover the bandwidth of the transducer. However, the transfer function of the transducer $h(t)$ is frequency-dependent. The spatial distribution function of the scatterers $z(t)$ is also dependent on the frequency because the scattering cross-sections of the scatterers are proportional to the fourth power of ultrasound frequency [25].The above issues imply that the IER is a frequency-dependent parameter, as supported by the results obtained from the tissue-mimicking phantom(See Figure 10). The C_1, C_2, and IER values were inversely proportional to the ultrasound frequency. The difference is that the IER performed better than the C_1 and C_2 image intensities in reducing the mean decreasing rate with frequency, although in principle its frequency dependence is an unavoidable property. According to observations on the results in Figure 10, the IER value dropped down when the frequency was larger than 5.5 MHz. In order to allow the IER characterizing tissues with a larger dynamic range, ultrasound frequencies lower than 5.5 MHz may be used.

On the other hand, noise is the other potential issue to influence the IER. The phantom results indicated that the gain independence of IER performs worse when the gain is small, as indicated by the results in Figure 8. This may be explained by the noise effect on EMD that has been clarified in the previous study [12]. In general, the sources of external noise are numerous and complex, which mainly originate from the environment and user operation such as electromagnetic fields, instrument switching, or personnel contacting. Internal noises come from the electronic components and conduction wires within a system that may be a summation of various noises including thermal noise, shot noise, flicker noise, partition noise, and burst noise [26]. Due to those external and internal noises respectively exhibiting different frequency characteristics, the white noise, the summation of noises from all aspects, is the most commonly encountered electrical noise that affects the characteristics of input and output signals [27]. Smaller gains easily generate significant white noise interference to affect the EMD outcomes. White noise has a large bandwidth (a uniform distribution for an ideal condition) and contains fluctuations at higher frequencies compared with those in the signal. Therefore, noise provides the signal waveform with additional local extrema, thereby altering the probability of detecting local extrema for large- and small-amplitude waveforms in the signals [12]. The waveforms for the large-amplitude oscillations exhibit a relatively steeper slope compared with the small-amplitude waveforms; thus, the extrema of noise may not be conspicuous in the signal. By contrast, for the small-amplitude waveforms, the extrema from noise may be conspicuous and detectable. In this condition, IMF contains severe mode-mixing effects to affect EMD of data [12,28]. As supported by the results in Figure 7, the IER decreased with decreasing the SNR (i.e., equivalently increasing the noise interference). Thus, a larger gain and any strategiesfornoise reductionare suggested to improve the measurement error of the IER.

6. Conclusions

In this study, we have proposed a gain-independent index (i.e., IER) based on the first and second IMF components (i.e., C_1 and C_2 images) obtained from EMD. The contributions of this study

are summarized below: (i) the theoretical demonstration showed that signal decomposition and normalization by using EMD can eliminate the gain effect from the IER; (ii) the experimental results indicated that the IER can describe the echogenicity and that its value is less affected by the gain factor; and (iii) the image intensities (C_1 and C_2) and the IER are frequency-dependent. However, the IER has advantages over the C_1 and C_2 intensities in reducing the mean decreasing rate with frequency. This means that using the IER to describe the echogenicity provides a relatively low degree of frequency dependence compared with using the image intensities for the same measurement purpose. The current findings reveal that the gain-independent measurement on the echogenicity is possible when signal decomposition and normalization techniques are applied to image data.

Acknowledgments: The authors would like to thank the anonymous reviewers for their valuable comments and suggestions. This work was supported by the Ministry of Science and Technology (Taiwan) under Grant No. MOST 103-2221-E-182-001-MY3 and by the Chang Gung Memorial Hospital (Linkou, Taiwan) under Grant Nos. CIRPD1E0022, CMRPD1F0311, and CMRPD1C0711.

Author Contributions: ZhuhuangZhou conducted theoretical analysis, performed experiments, and wrote the manuscript. WeiweiWu, ShuicaiWu and KebinJia conducted data analysis. Po-Hsiang Tsui conducted data analysis and wrote the manuscript. All authors read and approved the final manuscript.

Conflicts of Interest: The authors declare that they have no competing interests.

References

1. Fowlkes, J.B.; Strieter, R.M.; Downing, L.J.; Brown, S.L.; Saluja, A.; Salles-Cunha, S.; Kadell, A.M.; Wrobleski, S.K.; Wakefield, T.W. Ultrasound echogenicity in experimental venous thrombosis. *Ultrasound Med. Biol.* **1998**, *24*, 1175–1182. [CrossRef]
2. Kraus, R.A.; Gaisie, G.; Young, L.W. Increased renal parenchymal echogenicity: Causes in pediatric patients. *Radiographics* **1990**, *10*, 1009–1018. [CrossRef] [PubMed]
3. Tchelepi, H.; Ralls, P.W.; Radin, R.; Grant, E. Sonography of diffuse liver disease. *J. Ultrasound Med.* **2002**, *21*, 1023–1032. [CrossRef] [PubMed]
4. Mathiesen, U.L.; Franzén, L.E.; Aselius, H.; Resjö, M.; Jacobsson, L.; Foberg, U.; Frydén, A.; Bodemar, G. Increased liver echogenicity at ultrasound examination reflects degree of steatosis but not of fibrosis in asymptomatic patients with mild/moderate abnormalities of liver transaminases. *Dig. Liver Dis.* **2002**, *34*, 516–522. [CrossRef]
5. Hu, C.F.; Chen, C.P.; Tsai, W.C.; Hu, L.L.; Hsu, C.C.; Tseng, S.T.; Shau, Y.W. Quantification of skeletal muscle fibrosis at different healing stages using sonography:A morphologic and histologic study in an animal model. *J. Ultrasound Med.* **2012**, *31*, 43–48. [CrossRef] [PubMed]
6. Fontaine, I.; Bertrand, M.; Cloutier, G. A system-based approach to modeling the ultrasound signal backscattered by red blood cells. *Biophys. J.* **1999**, *77*, 2387–2399. [CrossRef]
7. Shankar, P.M. A general statistical model for ultrasonic backscattering from tissues. *IEEE Trans. Ultrason. Ferroelectr. Freq. Control* **2000**, *47*, 727–736. [CrossRef] [PubMed]
8. Dantas, R.G.; Costa, E.T.; Leeman, S. Ultrasound speckle and equivalent scatterers. *Ultrasonics* **2005**, *43*, 405–420. [CrossRef] [PubMed]
9. Huang, N.E.; Shen, Z.; Long, S.R.; Wu, M.C.; Shih, H.H.; Zheng, Q.; Yen, N.C.; Tung, C.C.; Liu, H.H. The empirical mode decomposition method and the Hilbert spectrum for nonlinear and non-stationary time series analysis. *Proc. R. Soc.Lond. A* **1998**, *454*, 903–995. [CrossRef]
10. Huang, N.E.; Shen, Z.; Long, S.R. A new view of nonlinear water waves:The Hilbert spectrum. *Annu. Rev. Fluid Mech.* **1999**, *31*, 417–457. [CrossRef]
11. Huang, N.E.; Wu, Z.H. A review on Hilbert-Huang transform:Method and its applications to geophysical studies. *Rev.Geophys.* **2008**, *46*. [CrossRef]
12. Tsui, P.H.; Chang, C.C.; Huang, N.E. Noise-modulated empirical mode decomposition. *Adv. Adapt. Data Anal.* **2010**, *2*, 25–37. [CrossRef]
13. Fang, J.; Wan, Y.L.; Chen, C.K.; Tsui, P.H. Discrimination between newly formed and aged thrombi using empirical mode decomposition of ultrasound B-scan image. *BioMed Res. Int.* **2015**, *2015*, 403293. [CrossRef] [PubMed]

14. Tsui, P.H.; Chang, C.C.; Chang, C.C.; Huang, N.E.; Ho, M.C. An adaptive threshold filter for ultrasound signal rejection. *Ultrasonics* **2009**, *49*, 413–418. [CrossRef] [PubMed]
15. Fujii, Y.; Taniguchi, N.; Akiyama, I.; Tsao, J.W.; Itoh, K. A new system for in vivo assessment of the degree of nonlinear generation using the second harmonic component in echo signals. *Ultrasound Med. Biol.* **2004**, *30*, 1511–1516. [CrossRef] [PubMed]
16. Wu, Z.; Huang, N.E.; Chen, X. The multi-dimensional ensemble empirical mode decomposition. *Adv. Adapt. Data Anal.* **2009**, *1*, 339–372. [CrossRef]
17. Bennett, M.; McLaughlin, S.; Anderson, T.; McDicken, N. Empirical mode decomposition and tissue harmonic imaging. *Ultrasound Med. Biol.* **2005**, *31*, 1051–1061. [CrossRef] [PubMed]
18. Huang, N.E.; Shen, S.S. *The Hilbert-Huang Transform and Its Applications*; World Scientific Publishing Company: Singapore, 2005.
19. Zhang, Y.; Gao, Y.; Wang, L.; Chen, J.; Shi, X. The removal of wall components in Doppler ultrasound signals by using the empirical mode decomposition algorithm. *IEEE Trans. Biomed. Eng.* **2007**, *54*, 1631–1642. [CrossRef] [PubMed]
20. Tsui, P.H.; Chang, C.C.; Ho, M.C.; Lee, Y.H.; Chen, Y.S.; Chang, C.C.; Huang, N.E.; Wu, Z.H.; Chang, K.J. Use of nakagami statistics and empirical mode decomposition for ultrasound tissue characterization by a nonfocused transducer. *Ultrasound Med. Biol.* **2009**, *35*, 2055–2068. [CrossRef] [PubMed]
21. Tsui, P.H.; Wan, Y.L.; Huang, C.C.; Wang, M.C. Effect of adaptive threshold filtering on ultrasonic nakagami parameter to detect variation in scatterer concentration. *Ultrason. Imaging* **2010**, *32*, 229–242. [CrossRef] [PubMed]
22. Liao, A.H.; Shen, C.C.; Li, P.C. Potential contrast improvement in ultrasound pulse inversion imaging using EMD and EEMD. *IEEE Trans. Ultrason. Ferroelectr. Freq. Control* **2010**, *57*, 317–326. [CrossRef] [PubMed]
23. Lin, S.C.; Li, P.C. Automatic contrast enhancement using ensemble empirical mode decomposition. *IEEE Trans. Ultrason. Ferroelectr. Freq. Control* **2011**, *58*, 2680–2688. [CrossRef] [PubMed]
24. Sadeghi, S.; Behnam, H.; Tavakkoli, J. Ultrasound elastography using empirical mode decomposition analysis. *J. Med. Signals Sens.* **2014**, *4*, 18–26. [PubMed]
25. Shung, K.K.; Thieme, G.A. *Ultrasonic Scattering in Biological Tissues*; CRC Press: Boca Raton, FL, USA, 1993.
26. András, A. *Electronic Noise*; McGraw-Hill: New York, NY, USA, 1982.
27. Chen, J.; Shi, Y.; Shi, S. Noise analysis of digital ultrasonic system and elimination of pulse noise. *Int. J. Press. Vessels Pip.* **1998**, *75*, 887–890. [CrossRef]
28. Wu, Z.; Huang, N.E. Ensemble empirical mode decomposition, a noise-assisted data analysis method. *Adv. Adapt. Data Anal.* **2009**, *1*, 1–41. [CrossRef]